Planar cell polarity signaling in the uterus directs appropriate positioning of the crypt for embryo implantation

Jia Yuan[a,1], Jeeyeon Cha[a,1,2], Wenbo Deng[a], Amanda Bartos[a], Xiaofei Sun[a], Hsin-Yi Henry Ho[b], Jean-Paul Borg[c,d], Terry P. Yamaguchi[e], Yingzi Yang[f], and Sudhansu K. Dey[a,3]

[a]Division of Reproductive Sciences, Cincinnati Children's Hospital Medical Center, Cincinnati, OH 45229; [b]Department of Cell Biology and Human Anatomy, University of California Davis School of Medicine, Davis, CA 95616; [c]Centre de Recherche en Cancérologie de Marseille, Aix-Marseille University, UM105, 3284 Marseille, France; [d]Paoli Calmettes, UMR7258 CNRS, U1068 INSERM, Cell Polarity, Cell Signalling and Cancer - Equipe Labellisée Ligue Contre le Cancer, F 13009 Marseille, France; [e]Cancer and Developmental Biology Laboratory, Center for Cancer Research, National Cancer Institute at Frederick, National Institutes of Health, Frederick, MD 21702; and [f]Department of Developmental Biology, Harvard School of Dental Medicine, Boston, MA 02115

Edited by R. Michael Roberts, University of Missouri-Columbia, Columbia, MO, and approved November 4, 2016 (received for review September 7, 2016)

Blastocyst implantation is a complex process requiring coordination of a dynamic sequence of embryo–uterine interactions. Blood vessels enter the uterus from the mesometrium, demarcating the uterus into mesometrial (M) and antimesometrial (AM) domains. Implantation occurs along the uterine longitudinal axis within specialized implantation chambers (crypts) that originate within the evaginations directed from the primary lumen toward the AM domain. The morphological orientation of crypts in rodent uteri was recognized more than a century ago, but the mechanism remained unknown. Here we provide evidence that planar cell polarity (PCP) signaling orchestrates directed epithelial evaginations to form crypts for implantation in mice. Uterine deletion of Vang-like protein 2, but not Vang-like protein 1, conferred aberrant PCP signaling, misdirected epithelial evaginations, defective crypt formation, and blastocyst attachment, leading to severely compromised pregnancy outcomes. The study reveals a previously unrecognized role for PCP in executing spatial cues for crypt formation and implantation. Because PCP is an evolutionarily conserved phenomenon, our study is likely to inspire implantation studies of this signaling pathway in humans and other species.

PCP | Vangl2 | embryo implantation | uterus | crypt

Effective reciprocal cross-talk between the receptive uterus and a competent blastocyst is critical for successful implantation (1). In nearly all mammals studied, the uterus differentiates into a receptive state timed appropriately with the migration of blastocysts into the uterus to initiate bidirectional communication for implantation. The receptive state is transient; in mice the uterus becomes receptive on day 4 of pregnancy (day 1 = vaginal plug) and refractory to implantation by the afternoon of day 5 (2). The coordinated actions of progesterone and estrogen regulate the proliferation and/or differentiation of major uterine cell types in a spatiotemporal manner to establish this brief window of receptivity for implantation. These changes involve an interplay of ovarian hormones, transcription factors, growth factors, morphogens, cytokines, and other signaling molecules. Aberrations or defects in any of these pathways may result in implantation failure or defective implantation, which propagates adverse ripple effects through the remaining course of gestation, compromising pregnancy outcomes (2–5).

Blood vessels enter the uterus from the mesometrium and delineate the uterus into mesometrial (M) and antimesometrial (AM) domains. In mice, blastocyst attachment occurs within specialized crypts (implantation chambers), which originate as epithelial evaginations from the main lumen at orderly spaced intervals at the AM domain. The formation of these directed evaginations is initiated on the morning of day 3, and they elongate by the afternoon of day 4 for blastocyst attachment and subsequent crypt formation in the evening along the Wnt5a gradient (6). Blastocyst attachment coincides with increased endometrial vascular permeability at the site of the attachment, which can be monitored by i.v. injection of a blue dye; distinct blue bands indicate sites of blastocyst attachment in the uterus (3, 7). On day 5, the blue bands are distinct, and the underlying stroma surrounding the implantation chamber begins to differentiate into decidual cells (decidualization) to create a favorable environment to support embryonic growth (2).

The unique architectural organization of crypts for blastocyst homing and attachment was first recognized in rodents more than a century ago and later by other investigators (8, 9). However, the mechanism by which epithelial evaginations are appropriately directed to form crypts at the AM domain for embryo homing and implantation remained unknown.

The regular spacing of luminal epithelial (LE) evaginations in preparation for implantation is reminiscent of the spatial patterning and directed morphogenetic movements resulting from planar cell polarity (PCP) signaling during embryogenesis (10, 11). PCP is essential for establishing spatial cues during organogenesis in multicellular tissues, directing actin-dependent morphogenetic cell movements to polarize structures in a wide range of settings,

Significance

Blastocyst implantation is a complex process that coordinates reciprocal embryo–uterine interactions. The uterus is demarcated by mesometrial (A)–antimesometrial (AM) domains; implantation occurs at regularly spaced intervals along the longitudinal axis of the AM pole, within specialized implantation chambers (crypts). The organized crypt formation in the rodent uterus was first observed in 1901, but the mechanism driving this phenomenon remained unknown. We found that planar cell polarity (PCP) signaling coordinates luminal epithelial evaginations toward the AM domain to form crypts for embryo homing and implantation in mice. Disruption of PCP signaling by inactivation of Vang-like protein 2, but not Vang-like protein 1, in the uterus disturbs the regular formation of epithelial evaginations and crypts, disrupting implantation and decidualization and severely compromising pregnancy outcomes.

Author contributions: J.Y., J.C., W.D., H.-Y.H.H., J.-P.B., and S.K.D. designed research; J.Y., J.C., W.D., A.B., X.S., and S.K.D. performed research; J.-P.B., T.P.Y., Y.Y., and S.K.D. contributed new reagents/analytic tools; J.Y., J.C., W.D., A.B., X.S., H.-Y.H.H., J.-P.B., T.P.Y., Y.Y., and S.K.D. analyzed data; and J.Y., J.C., H.-Y.H.H., and S.K.D. wrote the paper.

The authors declare no conflict of interest.

This article is a PNAS Direct Submission.

[1]J.Y. and J.C. contributed equally to this work.

[2]Present address: Department of Medicine, Vanderbilt University Medical Center, Nashville, TN 37232.

[3]To whom correspondence should be addressed. Email: sk.dey@cchmc.org.

This article contains supporting information online at www.pnas.org/lookup/suppl/doi:10.1073/pnas.1614946113/-/DCSupplemental.

including *Drosophila* wing hair (12) and mammalian neural development (13). Disturbances in PCP signaling produce developmental anomalies in neural tube closure, left–right asymmetry, and hair cell orientation in the inner ear (14–20). In humans, mutations or polymorphisms of PCP components are associated with an array of developmental defects including spina bifida, cardiac outflow malformations, and cystic renal disease (21–24).

Vertebrate core PCP components are highly conserved and include noncanonical Wnt family members, their Frizzled receptors, coreceptors (Ror1/Ror2), and membrane-bound signaling intermediaries (Celsr1, Vangl, Scribble, Fat/Dachous) as well as intracellular protein mediators (Dvl, Prickle). These mediators are intracellularly sorted and reside asymmetrically along the apicobasal axis of the cell, initiating spatial organization through cell–cell contacts (19).

Here we show that PCP components display unique uterine expression before and during embryo implantation and, moreover, that mice with uterine-specific deletion of *Vangl2* (*Vangl2*$^{d/d}$ mice) show abnormal uterine PCP activity with changes in the spatial distribution of other PCP components. These changes lead to aberrant LE evaginations with random distribution of glands within both the M and AM domains, resulting in severe subfertility. Interestingly, conditional deletion of both *Vangl1* and *Vangl2* (*Vangl1*$^{d/d}$ *Vangl2*$^{d/d}$) in the uterus mostly recapitulated the infertility phenotype seen in *Vangl2*$^{d/d}$ females, suggesting that Vangl2 is the predominant isoform in this role; *Vangl1*$^{d/d}$ females showed normal fertility. We also found that disrupted PCP signaling is associated with derailed Noggin–Bmp2 interaction. Finally, we observed that PCP signaling pathways converge on Dvl2 signaling, and aberrant PCP signaling conferred defective decidualization in the underlying stroma surrounding the implantation chamber, suggesting PCP's role in the initiation of this process. Taken together, these findings provide clear in vivo and in vitro evidence that PCP signaling is critical for the formation of the directed epithelial evaginations leading to the formation of the crypts required for optimal blastocyst homing, implantation, and decidualization in the mouse uterus.

Results

Uterine *Vangl2* Deletion Causes Defects in Epithelial Evaginations and Crypt Formation and Severely Compromises Pregnancy Outcome. Vangl2, a core PCP component, works in collaboration with Vangl1, Celsr1, Scribble (Scrib), Dvl2, Wnt5a, and ROR to execute PCP signaling (16, 25–27). Immunofluorescence (IF) staining using a highly specific Vangl2 antibody (28) reveals that Vangl2 is distinctly localized in luminal and glandular epithelial cells on days 4 and 5 (the days of uterine receptivity and implantation, respectively) and at relatively lower levels in surrounding endothelial cells and stromal cells adjacent to the epithelium (Fig. 1*A* and Fig. S1). We chose to use conditional uterine deletion of *Vangl2*, because looptail mice homozygous for *Vangl2* mutation have structural defects in the uterus, with imbibition of fluid into the lumen and defects in the vaginal opening, precluding studies of PCP on implantation (29). In contrast, mice with conditional uterine deletion of *Vangl2* (*Vangl2*$^{d/d}$) by *Cre* expression under the control of progesterone receptor (*Pgr-Cre*) have normal uterine structures and morphology; uterine deletion of Vangl2 was highly efficient (Fig. S1). However, *Vangl2*$^{d/d}$ females show severe subfertility: Approximately 46% of plug-positive females fail to produce any litters after multiple mating, and the remaining 54% of plug-positive *Vangl2*$^{d/d}$ females produce significantly smaller litters (Fig. 1*B*). These results show that Vangl2 is critical for normal fertility. A careful examination of fertility phenotypes showed that these females exhibited pregnancy stage-specific effects. *Vangl2*$^{d/d}$ females had numerous unevenly spaced resorption sites on days 12 and 14 of pregnancy (Fig. 1*C* and Fig. S2 *A* and *B*) preceded by retarded placental development with a predominance of trophoblast giant cells (TGC) and reduced expression of a TGC marker gene *Mash2* (Fig. S2*C*).

On day 8 of pregnancy, *Vangl2*$^{d/d}$ females showed an atypical morphology of the implantation sites: In comparison with the

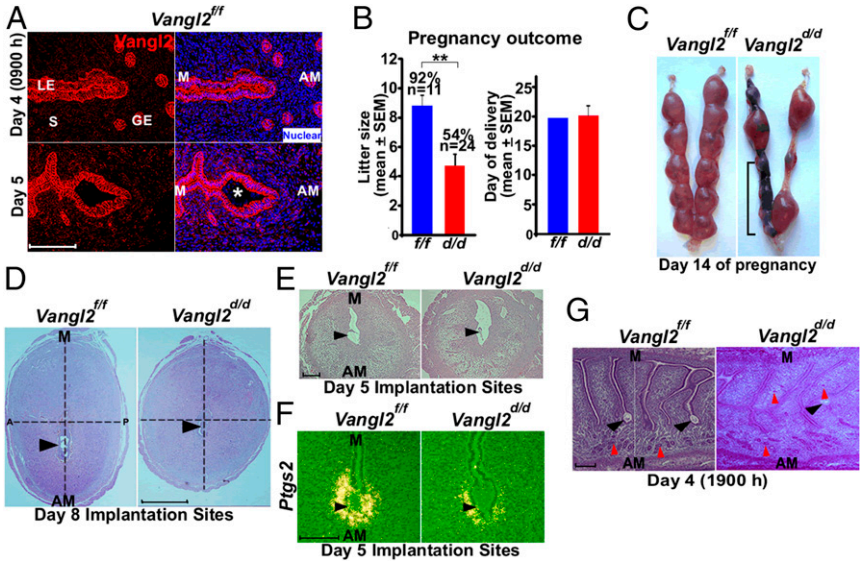

Fig. 1. Uterine inactivation of *Vangl2* results in compromised pregnancy outcome. (*A*) IF localization of Vangl2 in uteri on days 4 and 5 of pregnancy. GE, glandular epithelium; LE, luminal epithelium; S, stroma; *, embryo. (Scale bar, 100 μm.) (*B*) Litter sizes and day of delivery in littermate *Vangl2*$^{f/f}$ and *Vangl2*$^{d/d}$ females. Percentages and numbers above the bars indicate the number of litters born compared with the total number (*n*) of plug-positive females in each genotype. Data are shown as mean ± SEM; $^{**}P < 0.01$. (*C*) Day 14 implantation sites in *Vangl2*$^{f/f}$ and *Vangl2*$^{d/d}$ females. The bracket indicates adjacent resorption sites. (*D*) Histology of day 8 implantation sites in *Vangl2*$^{f/f}$ and *Vangl2*$^{d/d}$ mice. Note the elliptical vs. round shape of *Vangl2*$^{f/f}$ and *Vangl2*$^{d/d}$ implantation sites, respectively. (Scale bar, 1 mm.) A, anterior; P, posterior. (*E*) Histology of day 5 implantation sites in *Vangl2*$^{f/f}$ and *Vangl2*$^{d/d}$ mice. (Scale bar, 200 μm.) (*F*) In situ hybridization of *Ptgs2* in *Vangl2*$^{f/f}$ and *Vangl2*$^{d/d}$ implantation sites on day 5. (Scale bar, 100 μm.) (*G*) Histology of longitudinal sections of *Vangl2*$^{f/f}$ and *Vangl2*$^{d/d}$ uteri on the evening of day 4. The vertical line separates serial sections showing separate crypts from the same uterine piece. Black arrowheads indicate the location of embryos. Red arrowheads indicate glands. (Scale bar, 200 μm.)

normally elliptical implantation sites of *Vangl2*$^{f/f}$ females, which align with the embryonic axis, *Vangl2*$^{d/d}$ implantation sites were more spherical. The ratio of length along the M–AM axis respective to the anterior–posterior axis was 24% less in *Vangl2*$^{d/d}$ females (Fig. 1*D*), indicating abnormal implantation chamber development and pregnancy progression in these mice. These morphological changes suggested that adverse pregnancy effects in *Vangl2*$^{d/d}$ mice originated earlier. When examining the status of implantation sites on day 5 by blue dye injection (7), we often found very weak blue bands, indicating inferior blastocyst attachment in *Vangl2*$^{d/d}$ uteri (Fig. 1*E* and Fig. S2*D*). This finding was reinforced by the observation of aberrant cell-specific expression of *Ptgs2* (Cox2), a marker for successful implantation, on day 5 (Fig. 1*F*) (30).

To explore further LE evagination before blastocyst attachment on the evening of day 4, we examined the histology of uterine longitudinal sections. Normally, epithelial evaginations for crypt formation occur at regular intervals aligned with glands and are invariably directed toward the AM domain (Fig. 1*G*). We found that in *Vangl2*$^{d/d}$ females evaginations lack direction and are situated at both the M and AM domains, resulting in dysfunctional formation of crypts and defective attachment of the embryos positioned within these crypts on the evening of day 4 (Fig. 1*G*). Interestingly, this phenotype of severe subfertility in *Vangl2*$^{d/d}$ females was not caused by altered uterine receptivity, as evaluated by the expression of *Ihh* and *Msx1*, markers of uterine receptivity, on day 4 (Fig. S2*E*) (3) or by changes in epithelial cell proliferation (Fig. S2*F*). In addition, ovarian hormone levels, ovarian Vangl2 expression, and uterine expression of progesterone receptor (PR) and estrogen receptor (ER) showed no apparent changes in *Vangl2*$^{f/f}$ or *Vangl2*$^{d/d}$ mice (Fig. S3). Taken together, these results show a previously unrecognized role of uterine Vangl2 in the orientation of epithelial evaginations and crypt formation, because loss of this signaling in *Vangl2*$^{d/d}$ mice led to aberrant implantation and adverse pregnancy outcome.

PCP Activity Directs LE Evaginations to Form Crypts at the AM Domain. Vangl2 executes PCP signaling with Celsr1, Scrib, and Vangl1 as well as with intracellular protein mediators such as Dvl (28, 31–33). We focused on these PCP components because Vangl2 is known to interact directly with Scrib and Celsr1; we also confirmed the direct interaction of Scrib with Vangl2 (Fig. S4*A*). Spatiotemporal localization of PCP components shows that Vangl2 and Scrib are first substantially expressed in the LE with localization to the apical surface on day 3 of pregnancy (Fig. S4*B*) and are further amplified on day 4 before implantation (Fig. 1*A*), suggesting progesterone regulation of Vangl2 expression. This expression is similar to Wnt5a expression (6). To examine the spatial distribution of PCP proteins as a functional output of PCP

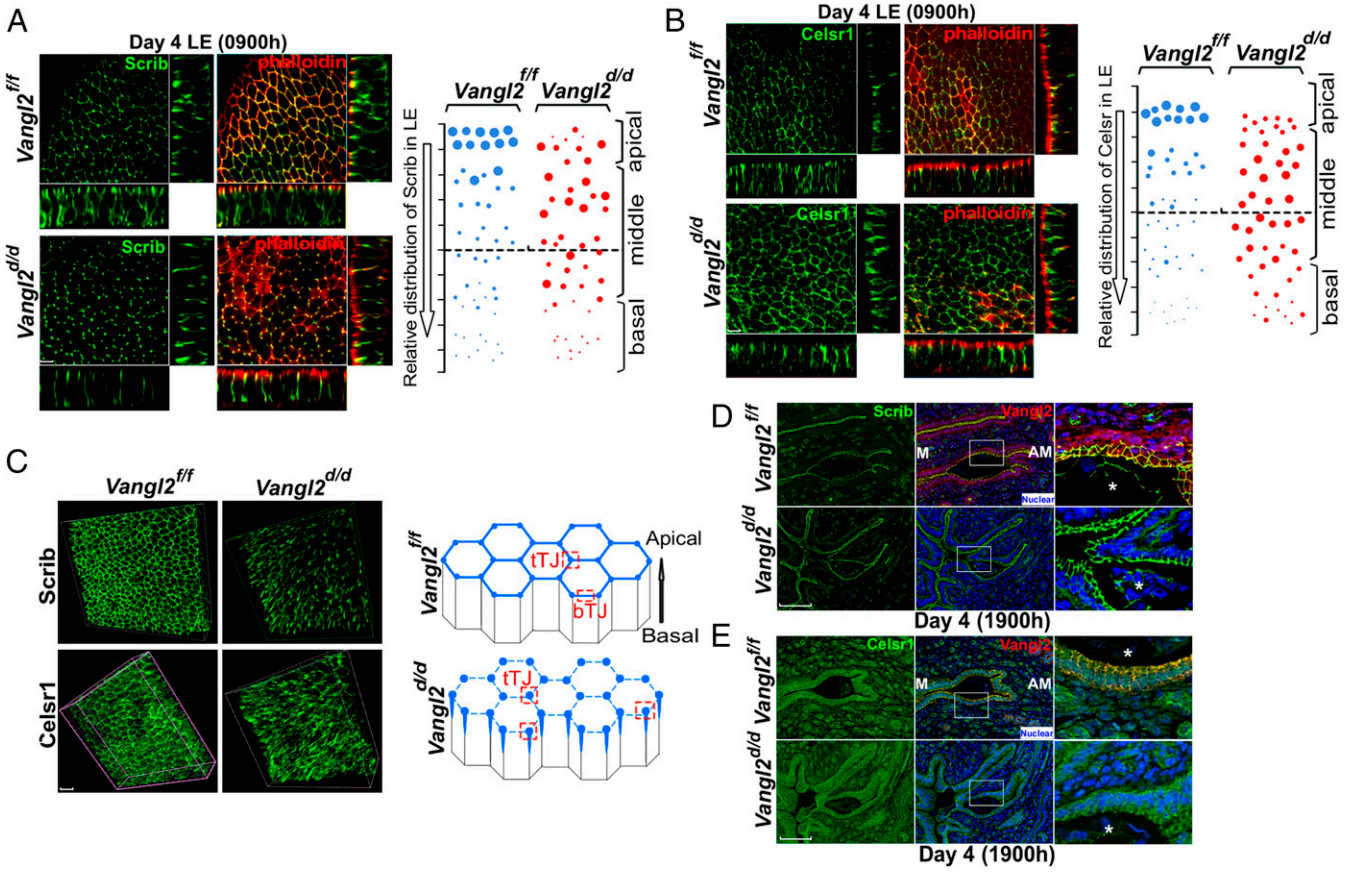

Fig. 2. Aberrant distribution of PCP proteins in *Vangl2*$^{d/d}$ luminal epithelia. (*A*, *Left*) 3D reconstruction of Scrib localization by IF in ex vivo explants of *Vangl2*$^{f/f}$ and *Vangl2*$^{d/d}$ uterine LE on day 4 showing that colocalization of Scrib and phalloidin was lost in *Vangl2*$^{d/d}$ LE cells. (Scale bar, 10 μm.) (*Right*) Relative apicobasal distribution of Scrib in *Vangl2*$^{f/f}$ and *Vangl2*$^{d/d}$ LE. (*B*, *Left*) 3D reconstruction of Celsr1 localization on the morning of day 4. (Scale bar, 10 μm.) (*Right*) Relative apicobasal distribution of Celsr1 in *Vangl2*$^{f/f}$ and *Vangl2*$^{d/d}$ LE. (*C*, *Left*) Merged 3D images of IF of Scrib and Celsr1 at the apical surface of *Vangl2*$^{f/f}$ and *Vangl2*$^{d/d}$ LE cells on the morning of day 4. (*Right*) Changes in Scrib and Celsr1 accumulation at the apical surface of *Vangl2*$^{f/f}$ and *Vangl2*$^{d/d}$ LE cells. Note that in floxed LE, Scrib and Celsr1 localize to bicellular (bTJ) and tricellular (tTJ) tight junctions, but they are assembled primarily in tricellular junctions in *Vangl2*$^{d/d}$ LE. (Scale bar, 10 μm.) (*D*) IF of Scrib in the longitudinal uterine sections of *Vangl2*$^{f/f}$ and *Vangl2*$^{d/d}$ mice on the evening of day 4. (Scale bar, 100 μm.) (*E*) IF of Celsr1 in the longitudinal uterine sections of *Vangl2*$^{f/f}$ and *Vangl2*$^{d/d}$ mice on the evening of day 4. (Scale bar, 100 μm.) Asterisks in *D* and *E* indicate the location of embryos.

activity, we performed 3D reconstruction of IF images of Vangl2, Scrib, and Celsr1 in isolated, intact LE. The results show that Scrib and Celsr1 are colocalized with Vangl2 at the apical surface in the epithelium on the morning of day 4 when LE evagination is in progress (Fig. 2 *A* and *B*). In contrast, Scrib and Ceslr1 are not appropriately localized in *Vangl2*$^{d/d}$ LE (Fig. 2 *A* and *B* and Movies S1–S4). We also found that these PCP components accumulate less at bicellular junctions and more at tricellular junctions in *Vangl2*$^{d/d}$ LE, with diffuse distribution of phalloidin staining (Fig. 2*C* and Movies S5–S8). These results prompted us to examine the status of Scrib and Celsr1 in the uterus on the evening of day 4 before blastocyst attachment. We found that the localization of these PCP components is strikingly altered in irregularly oriented evaginations and crypts in *Vangl2*$^{d/d}$ mice (Fig. 2 *D* and *E*).

Celsr1 is clearly displayed in the crypt epithelial cells of *Vangl2*$^{f/f}$ females on day 5, but localization is patchy in *Vangl2*$^{d/d}$ mice (Fig. 3*A*). However, Scrib becomes undetectable in the *Vangl2*$^{f/f}$ crypt epithelium, appearing instead in the basal lamina and underlying stroma, but is retained in the epithelium in *Vangl2*$^{d/d}$ mice (Fig. 3*B*). In contrast, the abnormal spatial distribution of Scrib is associated with increased protein levels and phosphorylation, as shown by gel shift assays (Fig. 3*C*). There is evidence that Scrib phosphorylation in transfected cells interferes with its apical localization (34). Collectively, PCP activity is consistently aberrant in *Vangl2*$^{d/d}$ uteri around the time of implantation, manifesting poorly coordinated epithelial evaginations and aberrant crypt formation and implantation. These results suggest that disorganization of apical Scrib and Ceslr1 in the absence of Vangl2 compromises the apical actin-myosin cytoskeleton and directional cues between cells required for the execution of proper LE evaginations toward the AM domain.

We speculated that LE tight junctions were also altered in these mice, and thus we assessed the distribution of the tight junction protein ZO-1. Although it is expressed uniformly in the *Vangl2*$^{f/f}$ LE on day 4, its distribution is heterogeneous with variable intensity and distribution in *Vangl2*$^{d/d}$ LE (Fig. 3*D*). In the same context, the tight junction protein Claudin 1 is expressed at the bottom region of the crypt in *Vangl2*$^{f/f}$ uteri but is expressed diffusely throughout the crypt epithelium around the blastocyst in *Vangl2*$^{d/d}$ mice on day 5 (Fig. 3*E*). These changes, along with changes in PCP components, are reflected in inefficient removal of the LE barrier surrounding the embryo in *Vangl2*$^{d/d}$ mice on day 6, as indicated by the mislocalization of E-cadherin and β-catenin (Fig. 3*F*).

***Vangl2* Is the Principal Isoform for Executing PCP Signaling in the Uterus.** We speculated that Vangl1, a Vangl family member that interacts via the same PDZ domain as Vangl2, compensates for the loss of Vangl2 to retain partial fertility in some *Vangl2*$^{d/d}$ females. This assumption is supported by the observation of elevated levels of Vangl1 by quantitative RT-PCR (qRT-PCR) in *Vangl2*$^{d/d}$ uteri on day 4 of pregnancy (Fig. 4*A*). Because we could not identify any authentic commercial Vangl1 antibody, we used RNAscope in situ hybridization to localize cell-specific expression of *Vangl1* transcripts and found that the distribution of *Vangl1* expression in the uterus is similar to that of Vangl2 (Fig. 4*B*). To provide genetic evidence, we generated mice with uterine-specific deletion of *Vangl1* (*Vangl1*$^{d/d}$), and determined that deletion was proficient (Fig. 4*C*). We then examined the fertility phenotypes

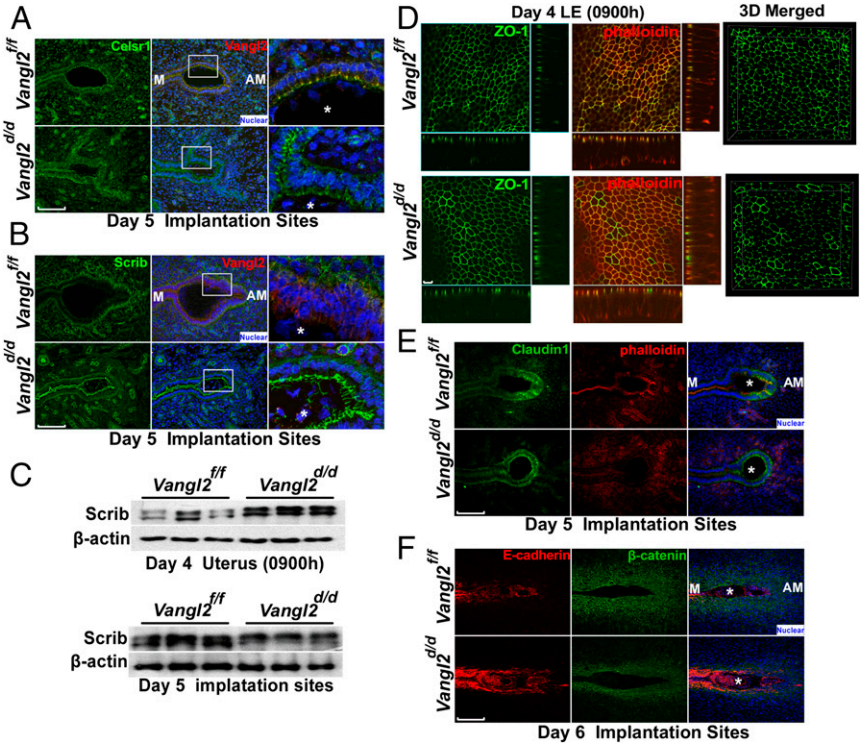

Fig. 3. Interactions among PCP components in the absence of Vangl2. (*A*) Celsr1 colocalizes with Vangl2 at the apical surface in *Vangl2*$^{f/f}$ implantation sites. In *Vangl2*$^{d/d}$ implantation sites Celsr1 localization was aberrant. (Scale bar, 100 μm.) (*B*) IF localization of Scrib and Vangl2 in day 5 implantation sites. Although Scrib was displayed at the apical side of the crypt epithelium in the *Vangl2*$^{d/d}$ mice, it was absent in *Vangl2*$^{f/f}$ females. (Scale bar, 100 μm.) (*C*) Western blotting for Scrib in day 4 uteri and day 5 implantation sites of *Vangl2*$^{f/f}$ and *Vangl2*$^{d/d}$ mice showed higher levels of Scrib and its phosphorylation in *Vangl2*$^{d/d}$ uteri. $n = 3$ females per genotype. (*D*, *Left*) The tight junction marker ZO-1 lost its uniform distribution at the apical surface of *Vangl2*$^{d/d}$ LE. (*Right*) 3D reconstruction of all layers. (Scale bars, 10 μm.) (*E*) IF of Claudin1 and phalloidin in day 5 implantation sites of *Vangl2*$^{f/f}$ and *Vangl2*$^{d/d}$ mice. (Scale bar, 100 μm.) (*F*) Poorly developed primary decidual zone with epithelial retention of E-cadherin and limited β-catenin consistent with inefficient invasion of the trophoblast through the crypt epithelium in *Vangl2*$^{d/d}$ mice. (Scale bar, 200 μm.) Asterisks in *A*, *B*, *E*, and *F* indicate the location of embryos.

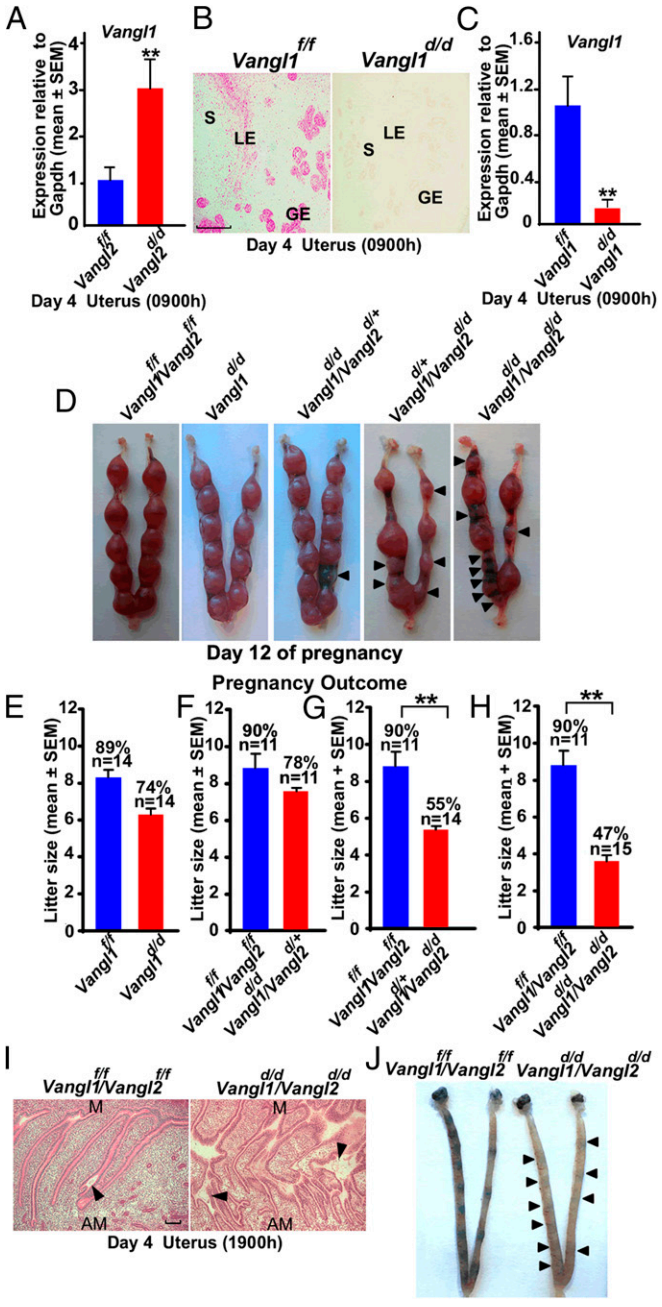

Fig. 4. Fertility phenotypes in *Vangl1*$^{d/d}$ mice and *Vangl1*$^{d/d}$*Vangl2*$^{d/d}$ mice. (*A*) Results of *Vangl1* qPCR in day 4 uteri of *Vangl2*$^{d/d}$ mice. $n = 3$; data are shown as mean ± SEM; $^{**}P < 0.01$. (*B*) In situ hybridization of *Vangl1* in *Vangl1*$^{f/f}$ and *Vangl1*$^{d/d}$ uteri on the morning of day 4 showing specific localization of *Vangl1* transcripts. Red granular speckles indicate transcripts. (Scale bar, 200 μm.) (*C*) qPCR results of *Vangl1* in day 4 uteri of *Vangl1*$^{f/f}$ and *Vangl1*$^{d/d}$ mice. Data are shown as mean ± SEM; $^{**}P < 0.01$. (*D*) Implantation sites in *Vangl1*$^{f/f}$*Vangl2*$^{f/f}$, *Vangl1*$^{d/d}$, *Vangl1*$^{d/d}$*Vangl2*$^{d/+}$, *Vangl1*$^{d/+}$*Vangl2*$^{d/d}$, and *Vangl1*$^{d/d}$*Vangl2*$^{d/d}$ mice on day 12. Arrowheads indicate degenerating embryos. (*E*) Litter sizes in littermate *Vangl1*$^{f/f}$ and *Vangl1*$^{d/d}$ females. Percentages and numbers above the bars indicate the number of litters born compared with the total number of plug-positive females (*n*) in each genotype. (*F–H*) Litter sizes in *Vangl1*$^{f/f}$*Vangl2*$^{f/f}$ and *Vangl1*$^{d/d}$*Vangl2*$^{d/+}$females (*F*), *Vangl1*$^{f/f}$*Vangl2*$^{f/f}$ females and *Vangl1*$^{d/+}$*Vangl2*$^{d/d}$ females (*G*), and *Vangl1*$^{f/f}$*Vangl2*$^{f/f}$ and *Vangl1*$^{d/d}$*Vangl2*$^{d/d}$ females (*H*). (*I*) Histology of longitudinal sections of day 4 uteri from *Vangl1*$^{f/f}$*Vangl2*$^{f/f}$ females and *Vangl1*$^{d/d}$*Vangl2*$^{d/d}$ females. Arrowheads indicate the location of embryos. (Scale bar, 500 μm.) (*J*) Implantation sites in *Vangl1*$^{f/f}$*Vangl2*$^{f/f}$ and *Vangl1*$^{d/d}$*Vangl2*$^{d/d}$ mice on day 5. Arrowheads indicate very weak bands in *Vangl1*$^{d/d}$*Vangl2*$^{d/d}$ mice.

in different crossings of mice with uterine deletions of *Vangl1* and/or *Vangl2*. The fertility phenotypes are normal in *Vangl1*$^{d/d}$ or *Vangl1*$^{d/d}$/*Vangl2*$^{d/+}$ females (Fig. 4 *D–F*), whereas the fertility phenotype in *Vangl1*$^{d/+}$/*Vangl2*$^{d/d}$ females closely resembles that of *Vangl2*$^{d/d}$ mice (Fig. 4 *D*, *G*, and *H*). However, the infertility rate is somewhat higher in *Vangl1*$^{d/d}$/*Vangl2*$^{d/d}$ females; 53% of plug-positive females were infertile, and the remaining 47% of plug-positive females generated smaller litters than *Vangl2*$^{d/d}$ females (Fig. 4*H*). Poor morphological coordination of LE evaginations for crypt formation is also apparent in day 4 uteri of *Vangl1*$^{d/d}$/*Vangl2*$^{d/d}$ females (Fig. 4*I*), with weak blue bands (implantation) on day 5 (Fig. 4*J*). This result is different from studies in other systems in which deletion of both isoforms led to more severe phenotypes than the deletion of *Vangl2* alone (27). The results suggest that Vangl2 is the predominant isoform critical for epithelial evaginations and crypt formation for implantation.

PCP Signaling Is Disrupted Under Aberrant Uterine Wnt5a–ROR Signaling. The failure of organized epithelial evaginations and crypt formation in *Vangl2*$^{d/d}$ females is reminiscent of the subfertility phenotypes observed in females with aberrant uterine Wnt5a–ROR signaling (6). Thus, we sought to examine the localization and activity of the major PCP components under altered Wnt5a–ROR signaling. To do so, we generated mice with uterine overexpression of Wnt5a (*Wnt5a*^{GOF}), uterine inactivation of Wnt5a (*Wnt5a*$^{d/d}$), and double deletion of *Ror1* and *Ror2* (*Ror1*$^{d/d}$/*Ror2*$^{d/d}$) using the *Pgr-Cre* driver (6). Single deletion of *Ror1* or *Ror2* showed no observable reproductive phenotypes (6). We found that the intensity of Vangl2 signaling correlates with the degree of Wnt5a–ROR signaling: In *Wnt5a*^{GOF} LE, Vangl2 localization is distinct in both the apical and basal sides of the LE, but the signal intensity is lower in *Wnt5a*$^{d/d}$ and *Ror1*$^{d/d}$/*Ror2*$^{d/d}$ females on the morning of day 4 (Fig. 5*A*). Similarly, signal intensities of Celsr1 and Scrib are aberrantly low in the crypt epithelia of *Wnt5a*$^{d/d}$ and *Ror1*$^{d/d}$/*Ror2*$^{d/d}$ uteri, but the intensity is appreciably higher in *Wnt5a*^{GOF} crypt epithelium on the evening of day 4 and the morning of day 5 (Figs. S5 and S6). This low signaling intensity was preceded by aberrant apical distribution of Vangl2, Scrib, and ZO-1 in the LE of *Wnt5a*$^{d/d}$, *Wnt5a*^{GOF}, and *Ror1*$^{d/d}$/*Ror2*$^{d/d}$ uteri on the morning of day 4 (Fig. 5 *B* and *C*). These findings show defective PCP activity in uteri with inappropriate Wnt5a–ROR signaling, providing evidence that Wnt5a–ROR signaling intersects PCP signaling in implantation.

Aberrant PCP Signaling Derails *Noggin–Bmp2* Interaction. The complex interactions between the embryo and uterus during implantation show common features of epithelial–mesenchymal interactions underlying developmental processes including limb, tooth, hair follicle, lung, and kidney development. Bone morphogenetic proteins (BMP) and their antagonists play a critical role in these processes (35–37). Noggin (Nog) is an antagonist to Bmp2 (38). We hypothesized that PCP signaling influences Nog–Bmp2 interaction to execute blastocyst attachment within the crypt. Using in situ hybridization, we examined the expression of *Bmp2* and *Nog*. In *Vangl2*$^{f/f}$ females *Nog* is expressed in the subepithelial stroma, but its expression is rapidly down-regulated, followed by *Bmp2* expression in the stroma at the site of embryo implantation before and after blastocyst attachment on the evening of day 4 and the morning of day 5. This pattern is disrupted in *Vangl2*$^{d/d}$ females during the same time periods (Fig. 6 *A* and *B*).

In pseudopregnant *Vangl2*$^{f/f}$ or *Vangl2*$^{d/d}$ females, generated by mating with vasectomized males, *Nog* expression is present in the subepithelial stroma along the entire length of the epithelial evagination, with no sign of *Bmp2* expression at the expected time of implantation. However, *Nog* expression is more robust in deleted uteri with aberrant epithelial evaginations (Fig. 6*C*). These results suggest that PCP signaling in the uterus is essential for implantation-competent blastocysts to confer down-regulation of *Nog* with induction of *Bmp2* to initiate the attachment reaction and subsequent decidualization at the implantation site.

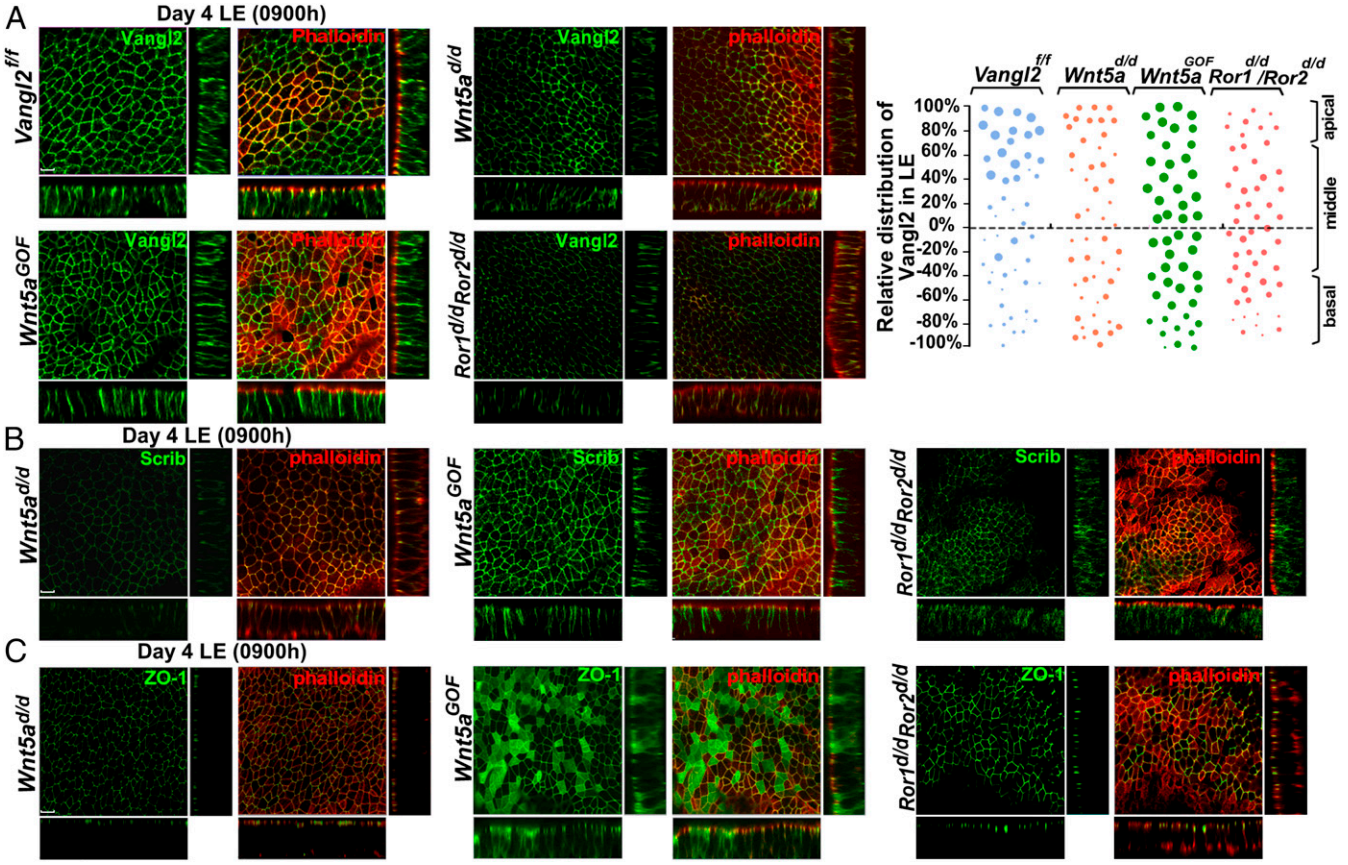

Fig. 5. Aberrant Wnt5a–ROR signaling dysregulates the localization of PCP components and tight junctions in LE. (*A*, *Left*) 3D reconstruction of Vangl2 IF showing aberrant expression patterns in *Wnt5a*$^{d/d}$, *Wnt5a*^{GOF}, and *Ror1*$^{d/d}$/*Ror2*$^{d/d}$ LE cells on the morning of day 4. (*Right*) Relative apicobasal distribution of Vangl2 in *Vangl2*$^{f/f}$ mice which was altered in *Wnt5a*$^{d/d}$, *Wnt5a*^{GOF}, and *Ror1*$^{d/d}$/*Ror2*$^{d/d}$ mice. (*B*) Comparison of aberrant apicobasal expression of Scrib in LE of *Wnt5a*$^{d/d}$, *Wnt5a*^{GOF}, and *Ror1*$^{d/d}$/*Ror2*$^{d/d}$ mice. (*C*) Aberrant apicobasal expression of ZO-1 in LE of *Wnt5a*$^{d/d}$, *Wnt5a*^{GOF}, and *Ror1*$^{d/d}$/*Ror2*$^{d/d}$ mice. (Scale bars, 10 μm.)

Bmp2 signaling was also shown to be critical for the initiation and progression of decidualization (38, 39). BMPs execute their effects by phosphorylating Smad proteins. We noted dampened BMP signaling, as indicated by reduced intensity of IF localization of pSmad1/5/8 in the primary decidual zone (pdz) on day 5 in *Vangl2*$^{d/d}$ females (Fig. 6*D*).

Dvl2 Signaling Is Dysregulated Under Abnormal PCP Signaling. Because PCP signaling can converge on the Dvl pathway, we explored the status of Dvl2 in the uterus under aberrant Wnt5a–ROR–Vangl2 signaling. Dvl2 is a scaffolding protein that interacts directly with Vangl2 and plays an important role downstream of PCP signaling (31). Western blotting results show that the levels of phosphorylated Dvl2 (pDvl2, active) are lower in *Vangl2*$^{d/d}$ uteri on the evening of day 4 with no apparent changes at the implantation site on day 5 (Fig. 7 *A* and *B*), although Dvl2 localization patterns in WT and *Vangl2*$^{d/d}$ uteri show little change on the evening of day 4 (Fig. S7*A*). We then asked if disturbances in Wnt5a–ROR signaling alter the Dvl2 phosphorylation status at the implantation sites. Indeed, levels of pDvl2 are very low to undetectable in *Wnt5a*$^{d/d}$ and *Ror1*$^{d/d}$ *Ror2*$^{d/d}$ uteri compared with those in WT uteri on the evening of day 4 and in day 5 implantation sites (Fig. 7 *C* and *E*–*G*). In contrast, *Wnt5a*^{GOF} mice show increased uterine pDvl2 levels on these days (Fig. 7 *C* and *D*). Phosphorylation was confirmed by treatment with calf intestinal alkaline phosphatase (CIAP) that abolished the phosphorylated band (Fig. 7*H*). Collectively, these results suggest that Wnt5a–ROR–PCP signaling converges on the downstream mediator Dvl2 in the uterus at the time of implantation. Studies in different systems showed that Wnt5a–ROR and Vangl2 signaling converge on Dvl2 activity for cell shape and cell-directed movements (10).

Aberrant PCP Signaling Resulted in Defective Decidualization. In mice, differentiating stromal cells surrounding the blastocyst initially form the pdz on day 5. This differentiation involves the transformation of stromal cells into epithelioid cells, which are densely packed to form an avascular zone around the implantation chamber. By day 6, the pdz is well formed, and a secondary decidual zone is formed at the periphery of the pdz. After day 8, placental and embryonic growth gradually reduce the decidual thickness. One proposed function of the pdz is to form a selective epithelioid barrier surrounding the embryo, safeguarding the embryo against harmful agents that may infiltrate from maternal circulation.

Because aberrant PCP activity interferes with BMP signaling, and because Bmp2 can influence Dvl2 distribution (40), we asked if Dvl2 activity is also associated with the initiation of decidualization (pdz formation). We examined Dvl2 localization by IF and found that Dvl2 accumulates in puncta within decidualizing stromal cells in the nascent pdz. Puncta density and Dvl2 IF intensity are markedly up-regulated in *Wnt5a*^{GOF} implantation sites on day 5, whereas *Wnt5a*$^{d/d}$ or *Ror1*/*Ror2*$^{d/d}$ pdz sites have significantly fewer puncta than those in WT mice (Fig. 7*I*). To explore the relationship between Dvl2 and Vangl2 in decidualization, IF of Dvl2 in stromal cells differentiating to decidual cells was examined. We found that Dvl2 is localized to distinct puncta in stromal cells differentiating to pdz at the implantation sites on day 5 in

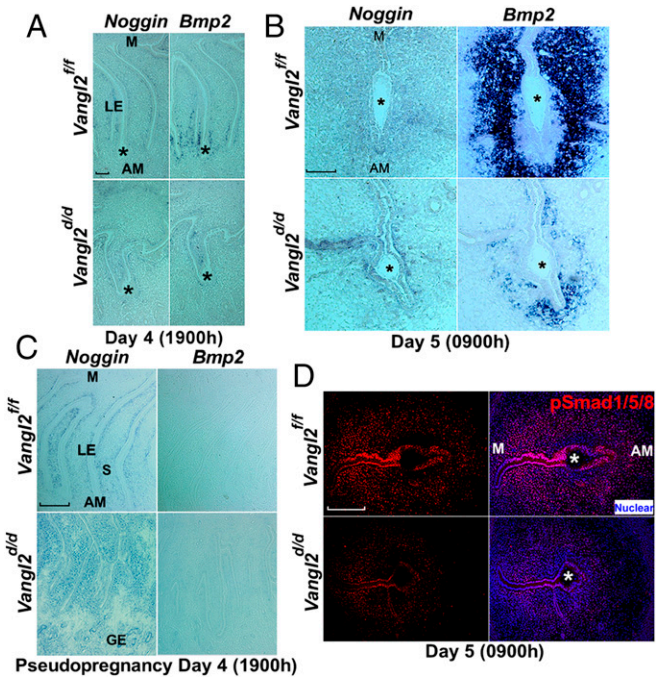

Fig. 6. Uterine deletion of *Vangl2* derails *Noggin* and *Bmp2* expression. (*A*) In situ hybridization of *Nog* and *Bmp2* in *Vangl2*$^{f/f}$ and *Vangl2*$^{d/d}$ uteri on the evening of day 4 showing their aberrant expression in *Vangl2*$^{d/d}$ uteri. (Scale bar, 200 μm.) (*B*) In situ hybridization of *Nog* and *Bmp2* in *Vangl2*$^{f/f}$ and *Vangl2*$^{d/d}$ implantation sites on day 5 showing the disappearance of *Nog* with robust *Bmp2* expression in *Vangl2*$^{f/f}$ females; this pattern was disrupted in *Vangl2*$^{d/d}$ implantation sites. (Scale bar, 100 μm.) (*C*) In situ hybridization of *Nog* and *Bmp2* in pseudopregnant *Vangl2*$^{f/f}$ uteri on the evening of day 4. Note *Nog* expression in the subepithelial stroma along the entire length of the LE evagination in *Vangl2*$^{f/f}$ and *Vangl2*$^{d/d}$ uteri, with more robust expression in the latter. *Bmp2* expression was not evident in *Vangl2*$^{f/f}$ and *Vangl2*$^{d/d}$ uteri. (Scale bar, 200 μm.) GE, glandular epithelium; LE, luminal epithelium; S, stroma. (*D*) IF of pSmad1/5/8 in *Vangl2*$^{f/f}$ and *Vangl2*$^{d/d}$ uteri. Asterisks indicate the location of the embryo.

Vangl2$^{f/f}$ females but is mostly absent from *Vangl2*$^{d/d}$ implantation sites (Fig. 7*J*). A greater abundance of puncta in the pdz cells is noted with the formation of the definitive pdz on day 6 in WT mice but not in conditionally deleted mice. These puncta are not evident when an antibody (105B), reported to detect the nonphosphorylated form of Dvl2 (41), is used (Fig. S7 *B* and *C*), suggesting that these puncta are positive for phosphorylated Dvl2.

Because puncta were abundant in pdz cells in vivo, we asked whether puncta are formed in stromal cells induced to decidualization in vitro. Primary stromal cells isolated from WT day 4 uteri were induced to decidualize in vitro (42). The decidual cells show higher pDvl2 levels than nondecidualized stromal cells in vitro (Fig. S7*D*), but they fail to show puncta formation. However, results with 10B5 Dvl2 antibody show lower levels in decidual cells in culture than in nondecidualized stromal cells (Fig. S7*E*). Although the definitive role of puncta is currently unknown (43–46), their formation in the uterus is clearly associated with the formation of the pdz. It is possible that puncta formation is relevant to the context of tissue patterning in vivo. Overall, these results suggest that PCP signaling is also involved in patterning stromal cells toward an epithelioid cell type during the pdz formation.

Discussion

Uterine receptivity is achieved primarily by the ovarian steroid hormones that provide an environment conducive to the complex molecular and physical interactions between the blastocyst trophectoderm and the uterine epithelium to achieve implantation. This study reveals a previously unrecognized but essential step in the receptive uterus before the attachment reaction: the morphological, cellular, and molecular changes that contribute to the formation of directed, regularly spaced LE evaginations and the formation of implantation chambers (crypts) at the AM domain. Previous studies had shown that aberrant uterine Wnt5a–ROR signaling caused defective implantation (6), but the mechanism by which Wnt5a–ROR signaling coordinates crypt formation remained unknown. Because Wnt5a forms a signaling gradient along the LE evaginations toward the AM domain (6), we speculated that directed cell movement of the epithelial evaginations through the stromal bed is guided by PCP signaling. Indeed, the present findings show that noncanonical Wnt5a–ROR signaling intersects with PCP signaling to initiate epithelial evaginations from the main LE toward the AM domain. This process is evident from our studies showing that uterine inactivation of *Vangl2* (*Vangl2*$^{d/d}$) disrupts directed epithelial evaginations. The crucial role of PCP in LE evaginations was reinforced further by aberrant spatial distribution and expression of the PCP components Scrib, Celsr1, and Dvl2 in *Vangl2*$^{d/d}$ uteri and by the poor, asymmetric sorting of PCP components in LE cells in the absence of Vangl2. Aberrant uterine PCP signaling with misdirected evaginations results in poor fertility, with intrauterine demise of embryos and reduced litter size.

This study uniquely identifies a physiologic role for PCP signaling in female fertility. This pathway has several roles during development, and we show here its requirement in maternal uterine tissues before and during implantation (Fig. S8). Mouse blastocysts do not express *Pgr-Cre* (3), eliminating the role of embryonic PCP in this event. Because this pathway is likely evolutionarily conserved across flies, worms, and mammals, the discovery of its role in the mouse uterus in providing directional cues for epithelial evagination and crypt formation at the AM domain is of paramount importance in implantation. Although the Vangl1 and Vangl2 proteins belong to the same family, and both manifest protein–protein interactions via the PDZ domain, Vangl2 appears to be the dominant isoform in the uterus that influences the pregnancy events, because Vangl2 deficiency shows a severe adverse fertility phenotype, whereas fertility is normal in *Vangl1*-deleted uteri.

A previous study used unauthenticated Vangl1 and Vangl2 antibodies to show cell-specific localization and used intraluminal injections of Vangl1 and Vangl2 antisense oligonucleotides in an unspecified volume of water to show their effects on implantation in mice (47). The authors concluded that uterine Vangl1 and Vangl2 are required for implantation, although both embryos and uterine cells were exposed to antisense oligos. Because the uterine luminal volume is merely 150–200 nL per horn around the time of uterine receptivity and implantation with the closure of LE, intraluminal infusion of solution is likely to distort epithelial morphology, cell polarity, and function (48). Furthermore, the intraluminal infusion exposes both the embryo and uterus to antisense oligonucleotides, making it difficult to delineate the roles of Vangl from the uterus versus Vangl from the embryo. Therefore, methodological and experimental design limitations raise concerns over these results, which are contrary to our findings derived using conditional knockout mouse models and authenticated antibodies with mechanistic information on uterine PCP signaling in pregnancy events.

Despite PCP's numerous functions in developmental processes, such as embryogenesis and organogenesis, its function in implantation was unknown. We now show that PCP signaling is a potential mechanism underlying this process. In most mammals, the uterus houses and supports a growing embryo throughout pregnancy until parturition; embryo implantation is the seed of embryogenesis and is a crucial, beginning step in development. In this context, *Vangl2* transcripts in developing neonatal uteri from conditionally deleted *Wnt7a* mice were reduced showing poor adenogenesis (49).

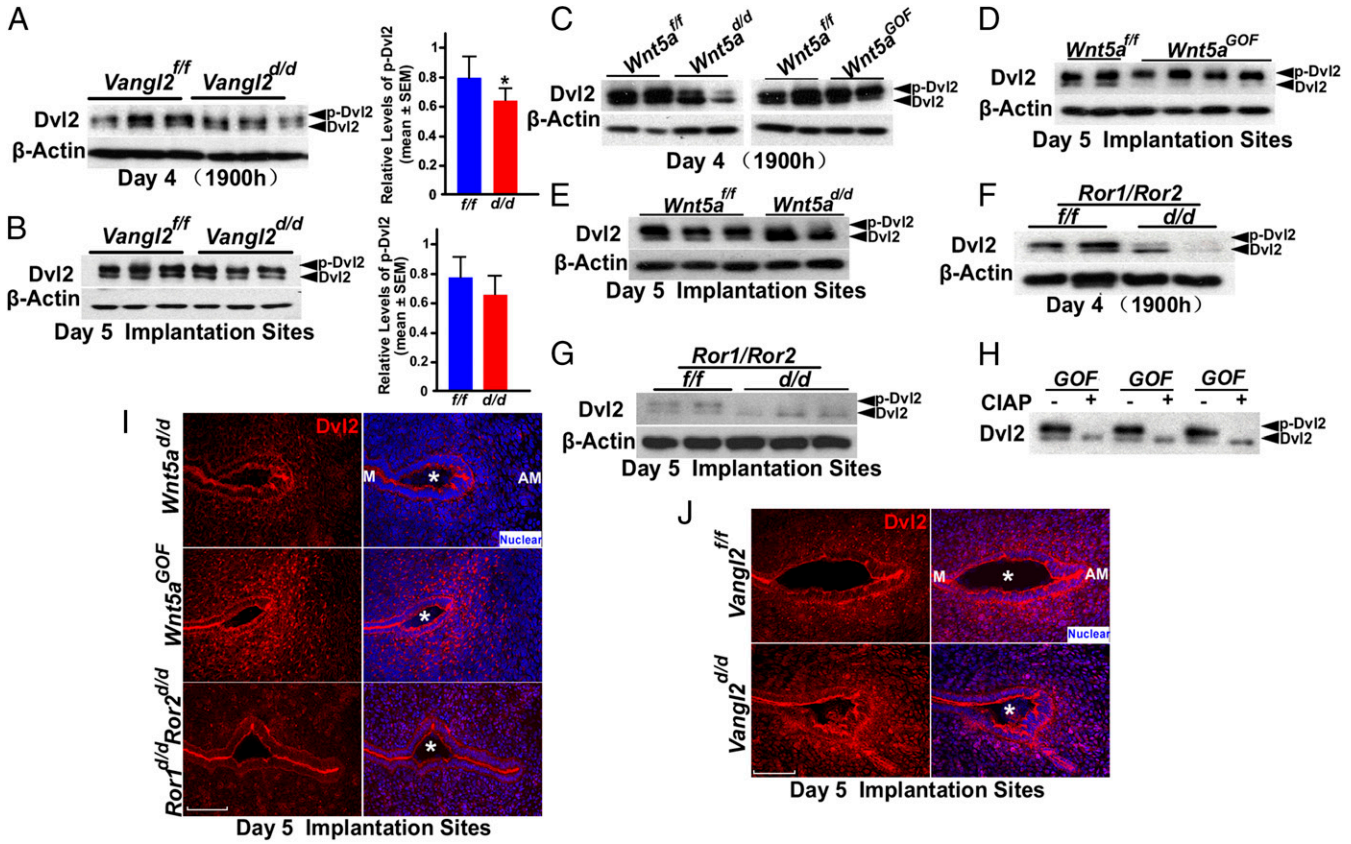

Fig. 7. Wnt5a–ROR–Vangl2 signaling pathways influence Dvl2 levels and activity during implantation. (*A* and *B*, *Left*) Western blotting results of Dvl2 in day 4 uteri (*A*) and day 5 implantation sites (*B*) of *Vangl2*$^{f/f}$ and *Vangl2*$^{d/d}$ mice. (*Right*) Relative levels of pDvl2. Data are shown as mean ± SEM; *$P < 0.05$. (*C*) Results of Western blotting of Dvl2 in day 4 uteri of *Wnt5a*$^{d/d}$ and *Wnt5a*^{GOF} mice. (*D* and *E*) Western blotting for Dvl2 in day 5 implantation sites of *Wnt5a*^{GOF} (*D*) and *Wnt5a*$^{d/d}$ (*E*) mice. (*F* and *G*) Western blotting for Dvl2 in day 4 uteri (*F*) and day 5 implantation sites (*G*) of *Ror1*$^{f/f}$/*Ror2*$^{f/f}$ and *Ror1*$^{d/d}$/*Ror2*$^{d/d}$ mice. (*H*) CIAP treatment of *Wnt5a*^{GOF} uterine samples leads to undetectable levels of phosphorylated Dvl2. (*I*) Dvl2 localization in *Wnt5a*$^{d/d}$, *Wnt5a*^{GOF}, and *Ror1*$^{d/d}$/*Ror2*$^{d/d}$ mice in day 5 implantation sites. (Scale bar, 100 μm.) (*J*) Dvl2 localization in *Vangl2*$^{f/f}$ and *Vangl2*$^{d/d}$ in crypt epithelium on day 5. (Scale bar, 100 μm.) Asterisks indicate the location of embryos.

Bmp2 signaling is localized primarily to stromal cells surrounding the attaching blastocyst and increases further during decidualization (38). Our observation of reduced expression of pSmad in the stroma in *Vangl2*$^{d/d}$ uteri on day 5, at the time of implantation and decidualization, suggests that this process is compromised in the uterus deficient in PCP signaling. This observation implies that epithelial–mesenchymal interactions in the context of implantation and decidualization involve PCP–BMP signaling. Previous work showing the role of BMP in embryo spacing (38) suggests that BMP signaling depends on Vangl2 signaling in regular spacing of the LE evaginations and crypt formation for implantation and then decidualization. Our observation that *Nog* disappears with the induction of *Bmp2* in the uterus before and after the initiation of implantation suggests that the Noggin–BMP2 interaction is tightly coupled with blastocyst attachment. The disruption of this interaction in the *Vangl2*$^{d/d}$ uterus points toward an intimate association of Noggin–BMP interactions with PCP activity. Indeed, there is evidence that *Nog* expression is tightly coupled with hair follicle development, in which PCP signaling is also a dominant feature (50). The definitive mechanism by which this *Nog–Bmp2* engagement is realized remains to be discovered.

Although epithelial–mesenchymal interactions are critical for the execution of many uterine events, it is not yet understood how stromal cells help LE evaginations form implantation chambers and then initiate decidualization following implantation. The distinct architectural arrangement of differentiating stromal cells to epithelioidlike cells with the acquisition of epithelial markers such as ZO-1 surrounding the implanting blastocyst to form the pdz is the hallmark of the decidualization process in rodents (2, 51). Subepithelial stromal cells surrounding the blastocyst express Vangl2, raising the possibility that PCP activity patterns stromal cells to acquire epitheliumlike characteristics at the site of implantation to initiate the pdz formation. The appearance of puncta as shown by pDvl2 localization in the pdz cells in vivo on day 5 is interesting and suggests that pDvl2 has a role in puncta formation that could serve as a marker for transitioning stromal cells to epithelioid cells in vivo. The absence of puncta in cells decidualized in vitro suggests that these decidual cells have lost the characteristics of pdz cells. The role of Dvl2 puncta has yet to be elucidated despite its identification in several systems (46, 52–54).

Our findings have uncovered a previously unidentified but critical role of PCP signaling to direct epithelial evaginations at regular intervals toward the AM domain for crypt formation and successful implantation. This finding is particularly interesting because severe subfertility in mice with aberrant PCP signaling is independent of altered uterine receptivity and steroid hormonal changes, providing evidence that PCP orchestrates LE evaginations to form implantation chambers for blastocyst homing and implantation. This study provides evidence for a physiological role for PCP signaling in the dynamically active adult mouse uterus. Whether this signaling is active in the human endometrium or in mammals other than rodents during implantation is not known. There is indication of undulation of the epithelium at the site of

the embryo implantation in human (Carnegie collections, plate 41) (55). Determining whether this undulation represents epithelial evagination is hampered by the availability of very few samples with limited details on early stages of pregnancy. Furthermore, research to identify very early stages of implantation in humans has been limited by ethical restrictions, and rightfully so. Therefore, the presence of epithelial evagination/undulation before blastocyst attachment is yet to be experimentally documented. Nonetheless, the human endometrium undergoes profound epithelial cell-surface changes with the formation of pinopode (uterodome) and with changes in surface microvilli and cilia during the endometrial receptive phase for implantation (56, 57). It is possible that PCP activity participates in these processes (58, 59). In addition, the formation of epithelial plaque at the site of embryo implantation in humans and, more noticeably, in subhuman primates (macaque) (60) suggests the possible participation of PCP signaling. Thus, the knowledge derived from this study in mice will encourage basic scientists and clinical investigators to probe for PCP signaling in implantation events in humans and other species. This signaling is particularly relevant to investigations of the cause of abnormal implantation in multiple-gestation pregnancies in humans and placenta previa, a source of significant mortality and/or morbidity of the mother and fetus (61, 62). The proteome atlas showing the expression of major PCP components including Vangl2, Vangl1, Scrib, ROR, and Wnt5a in the human endometrium (63) suggests the involvement of PCP signaling in human implantation. Taken together, our research addresses a mechanism behind a long-standing observation in rodent implantation and can spur further studies on PCP signaling in the human uterus and other mammals to improve our understanding of how embryos are directed to select a uterine site for implantation.

Materials and Methods

Mice. *Pgr*$^{Cre/+}$, *Wnt5a*$^{d/d}$, *Wnt5a*^{GOF}, and *Ror1*$^{d/d}$*Ror2*$^{d/d}$ mouse lines were generated as previously described (6, 11, 64, 65). *Vangl1*$^{d/d}$, *Vangl2*$^{d/d}$, and *Vangl1*$^{d/d}$/*Vangl2*$^{d/d}$ mice were generated by mating floxed females with *Pgr*$^{Cre/+}$ males (3). *Vangl2* floxed mice were generated in Y.Y.'s laboratory (NIH), and *Vangl1* floxed mice were purchased from Jackson Laboratories. All mice used in this study were housed under a constant 12-h/12-h light/dark cycle in the Cincinnati Children's Animal Care Facility according to NIH and institutional guidelines for the use of laboratory animals. All protocols were approved by the Cincinnati Children's Animal Care and Use Committee. Mice were provided with autoclaved Laboratory Rodent Diet 5010 (Purina) and UV light-sterilized reverse osmosis/deionized constant-circulation water ad libitum.

Analysis of Pregnancy Events. Female mice were mated with littermate floxed males to induce pregnancy. Ovulation, fertilization, preimplantation embryo development, and implantation were assessed as previously described (3). The morning of finding the vaginal plug was considered day 1 of pregnancy. To examine uterine receptivity and implantation, pregnant dams were killed on day 4 (0900–1000 h), and day 5 (0900 h), respectively. Implantation sites were visualized by i.v. injection of a Chicago blue dye solution before mice were killed, and the number of implantation sites demarcated by distinct blue bands was recorded. The number of blue bands on day 5 in control and experimental animals was compared as an index of ovulation, fertilization, and oviductal embryo transport and development. For litter size analysis, pregnant females were monitored from days 17–21 by observing mice daily for parturition and litter size.

Immunohistochemistry and Histology. Immunohistochemistry of ER (sc-542; Santa Cruz Biotechnology) and PR (8757; Cell Signaling Technology) was performed in paraffin-embedded sections using specific antibodies. Tissue sections from control and experimental groups were processed on the same slide. A Histostain-Plus (diaminobenzidine) kit (859243; Thermo Scientific) was used to visualize specific antigens. Paraffin sections (6 μm) were deparaffinized, hydrated, and stained with H&E for light microscopy analysis (3).

IF and Confocal Microscopy. IF for Vangl2 (custom generated in the J.-P.B. laboratory, INSERM), ZO-1 (33-9100; Thermo Scientific), rabbit E-cadherin (3195s; Cell Signaling Technology), goat E-cadherin (sc-31020; Santa Cruz Biotechnology), β-catenin (sc-1496; Santa Cruz Biotechnology), Claudin 1 (71-7800; Thermo Scientific) and phalloidin (43166A; Thermo Scientific), Scrib (H300; Santa Cruz Biotechnology), Celsr1 (custom generated in the Fuchs laboratory, Rockefeller University, New York), phospho-Smad1/Smad5/Smad8 antibody (generated by Dan Vasiliauskas, Susan Morton, Tom Jessell, and Ed Laufer, Columbia University, New York), Dvl2 (bs-9059R; Bioss Antibodies), Ki67 (RM-9106-S; Thermo Scientific), and 10B5 (sc-8026; Santa Cruz) was performed using secondary antibodies conjugated with Cy-2, Cy-3, or Cy-5 (Jackson ImmunoResearch). Nuclear staining was performed using Hoechst 33342. Tissue sections from control and experimental groups were processed onto the same slide.

Whole-Mount LE Recovery and Immunostaining. Uteri were cut into 2- to 3-mm pieces and were incubated in HBSS containing 120 mg/mL dispase and 125 mg/mL pancreatin. The pieces were incubated at 37 °C for 1 h. The intact LE then was gently squeezed out of the uterus by a small pair of forceps. The isolated LE was fixed in 4% (wt/vol) paraformaldehyde (PFA) for 10 min at room temperature, washed gently three times in PBS, and then subjected to IF as described above. The *z* axis and *x*, *y* axes were set up for IF scanning by a Nikon A1 invert confocal microscope, and Imaris software was used to analyze the images. At least two independent samples were analyzed.

RNA Isolation and qPCR. RT-PCR was performed as described (3), using the following primers: 5′-CCAAACAGCAGCCTTACCAT-3′ and 5′-TCCTTAAGCCCATTGGTCAC-3′ for *Vangl2* (product size 196 bp); 5′-TGGAGGGTAATGTCACAGCA-3′ and 5′-AAACCGTTCTTTGCCCTTCT-3′ for *Vangl1* (product size 200 bp); and 5′-TCCATGACAACTTTGGCATTG-3′ and 5′-CAGTCTTCTGGGTGGCAGTGA-3′ for mouse *Gapdh* (product size, 72 bp). *Gapdh* served as an internal control.

In Situ Hybridization. PFA-fixed frozen sections from control and experimental groups were processed onto the same slide and hybridized with ^{35}S-labeled cRNA probes (3, 30) or were hybridized with digoxigenin (DIG)-labeled cRNA probes. DIG-labeled probes were generated according to the manufacturer's protocol (Roche). RNAscope in situ hybridization was performed as described (66). Briefly, frozen tissue sections were fixed in 4% PFA/PBS and then were incubated with hydrogen peroxide and Protease IV according to the manufacturer's protocol (Advanced Cell Diagnostics, ACD). The slides then hybridized with the *Vangl1* probe generated by ACD at 40 °C for 2 h. After hybridization, slides were subjected to signal amplification using an HD 2.0 Detection Kit (ACD).

Immunoblotting. Antibodies used included Vangl2 (J.-P.B.), and Actin (sc-1615; Santa Cruz Biotechnology). Bands were visualized using an ECL kit (RPN2108; GE Healthcare). Actin served as a loading control. For the gel-shift assay, proteins were separated in 10% Bis-acrylamide gel for 4 h at 70 V (for Vangl2) or 7% Bis-acrylamide gel for 4 h at 70 V (for Dvl2). For phosphatase treatment, *Wnt5a*^{GOF} implantation sites were homogenized in RIPA buffer as described above, and an aliquot of each sample was treated with calf intestine alkaline phosphatase (CIAP), 1 unit/μg protein, for 40 min at 37 °C. Vangl2 and Dvl2 proteins were examined by immunoblotting.

Primary Stromal Cell Culture. Uteri from day 4 pseudopregnant WT mice were split open longitudinally and cut into small pieces (2–3 mm long). Tissue pieces were incubated with pancreatin and dispase for 1 h on ice, followed by 30 min at room temperature and 10 min at 37 °C. Fragments of LE sheets were liberated by pipetting the digests several times. The remaining tissue fragments were incubated in type II collagenase to free stromal cells. Stromal cells were suspended in DMEM:F12 Nutrient Mixture (DMEM:F12) containing 10% heat-inactivated charcoal-stripped FCS, 50 units/mL penicillin, 50 μg/mL streptomycin, and 1.25 μg/mL fungizone. Cell suspensions were filtered through a 70-μm nylon mesh to remove glands and clumps of epithelial cells. Stromal cells were plated in 3.5-mm Petri dishes and allowed to attach for 48 h at 37 °C in 5% CO_2 in air. Protein lysates were collected 24 h later in RIPA buffer for immunoblotting.

In Vitro Decidualization. Stromal cells from day 4 of pregnancy were collected by enzymatic digestion as described previously (67). The cells were cultured overnight before the initiation of decidualization by treatment with estradiol-17β (10 nM) and progesterone (1 μM) in phenol-red free DMEM/F12 medium supplemented with charcoal-stripped 1% FBS (wt/vol).

Measurement of Serum Estradiol-17β and Progesterone Levels. Sera were collected on days 4, 8, and 12 of pregnancy, and hormone levels were measured by enzyme immunoassay kits (Cayman) (4).

Statistics. Statistical analyses were performed using a two-tailed Student's *t* test. A value of $P < 0.05$ was considered statistically significant.

ACKNOWLEDGMENTS. We thank Katie A. Gerhardt for efficient editing and preparation of the manuscript; Yingju Li for help in some histological sectioning; Alexandra Tavenier for help in genotyping; Elaine Fuchs (Rockefeller University) and Ed Laufer (Columbia University) for kindly providing the Celsr1 and pSmad1/5/8 antibodies, respectively; and Matt Kofron for support with confocal imaging at the Cincinnati Children's Nikon Center of Excellence in Imaging and Services. This work was supported in part by NIH Grants R01HD068524, DA006668, and P01CA77839 and by grants from the March of Dimes (to S.K.D.). J.C. was the recipient of National Research Service Fellow Award F30AG040858 of the University of Cincinnati Medical Scientist Training Program.

1. Wang H, Dey SK (2006) Roadmap to embryo implantation: Clues from mouse models. *Nat Rev Genet* 7(3):185–199.
2. Cha J, Sun X, Dey SK (2012) Mechanisms of implantation: Strategies for successful pregnancy. *Nat Med* 18(12):1754–1767.
3. Daikoku T, et al. (2011) Conditional deletion of Msx homeobox genes in the uterus inhibits blastocyst implantation by altering uterine receptivity. *Dev Cell* 21(6):1014–1025.
4. Hirota Y, et al. (2010) Uterine-specific p53 deficiency confers premature uterine senescence and promotes preterm birth in mice. *J Clin Invest* 120(3):803–815.
5. Song H, et al. (2002) Cytosolic phospholipase A2alpha is crucial [correction of A2alpha deficiency is crucial] for 'on-time' embryo implantation that directs subsequent development. *Development* 129(12):2879–2889.
6. Cha J, et al. (2014) Appropriate crypt formation in the uterus for embryo homing and implantation requires Wnt5a-ROR signaling. *Cell Reports* 8(2):382–392.
7. Psychoyos A (1973) Endocrine control of egg implantation. *Handbook of Physiology*, eds Greep EGARO, Geiger SR (American Physiology Society, Washington, DC), pp 187–215.
8. Enders AC, Schlafke S, Welsh AO (1980) Trophoblastic and uterine luminal epithelial surfaces at the time of blastocyst adhesion in the rat. *Am J Anat* 159(1):59–72.
9. Burckhard G (1901) Die Implantation des Eies der Maus in die Uterusschleimhaut und die Umbildung derselben zur Decidua. *Archiv für mikroskopische Anatomie* 57(3):528–569.
10. Gao B, et al. (2011) Wnt signaling gradients establish planar cell polarity by inducing Vangl2 phosphorylation through Ror2. *Dev Cell* 20(2):163–176.
11. Ho HY, et al. (2012) Wnt5a-Ror-Dishevelled signaling constitutes a core developmental pathway that controls tissue morphogenesis. *Proc Natl Acad Sci USA* 109(11):4044–4051.
12. Hogan J, Valentine M, Cox C, Doyle K, Collier S (2011) Two frizzled planar cell polarity signals in the Drosophila wing are differentially organized by the Fat/Dachsous pathway. *PLoS Genet* 7(2):e1001305.
13. Park TJ, Mitchell BJ, Abitua PB, Kintner C, Wallingford JB (2008) Dishevelled controls apical docking and planar polarization of basal bodies in ciliated epithelial cells. *Nat Genet* 40(7):871–879.
14. Collu GM, Mlodzik M (2015) Planar polarity: Converting a morphogen gradient into cellular polarity. *Curr Biol* 25(9):R372–R374.
15. Devenport D, Oristian D, Heller E, Fuchs E (2011) Mitotic internalization of planar cell polarity proteins preserves tissue polarity. *Nat Cell Biol* 13(8):893–902.
16. Gao B, Yang Y (2013) Planar cell polarity in vertebrate limb morphogenesis. *Curr Opin Genet Dev* 23(4):438–444.
17. Gray RS, Roszko I, Solnica-Krezel L (2011) Planar cell polarity: Coordinating morphogenetic cell behaviors with embryonic polarity. *Dev Cell* 21(1):120–133.
18. Olofsson J, Axelrod JD (2014) Methods for studying planar cell polarity. *Methods* 68(1):97–104.
19. Sebbagh M, Borg JP (2014) Insight into planar cell polarity. *Exp Cell Res* 328(2):284–295.
20. van Amerongen R, Nusse R (2009) Towards an integrated view of Wnt signaling in development. *Development* 136(19):3205–3214.
21. Goggolidou P (2014) Wnt and planar cell polarity signaling in cystic renal disease. *Organogenesis* 10(1):86–95.
22. Lei Y, et al. (2013) Mutations in planar cell polarity gene SCRIB are associated with spina bifida. *PLoS One* 8(7):e69262.
23. Wu G, Huang X, Hua Y, Mu D (2011) Roles of planar cell polarity pathways in the development of neural [correction of neutral] tube defects. *J Biomed Sci* 18:66.
24. Wu G, Ge J, Huang X, Hua Y, Mu D (2011) Planar cell polarity signaling pathway in congenital heart diseases. *J Biomed Biotechnol* 2011:589414.
25. Devenport D (2014) The cell biology of planar cell polarity. *J Cell Biol* 207(2):171–179.
26. Oishi I, et al. (2003) The receptor tyrosine kinase Ror2 is involved in non-canonical Wnt5a/JNK signalling pathway. *Genes Cells* 8(7):645–654.
27. Song H, et al. (2010) Planar cell polarity breaks bilateral symmetry by controlling ciliary positioning. *Nature* 466(7304):378–382.
28. Belotti E, et al. (2012) Molecular characterisation of endogenous Vangl2/Vangl1 heteromeric protein complexes. *PLoS One* 7(9):e46213.
29. Vandenberg AL, Sassoon DA (2009) Non-canonical Wnt signaling regulates cell polarity in female reproductive tract development via van gogh-like 2. *Development* 136(9):1559–1570.
30. Lim H, et al. (1997) Multiple female reproductive failures in cyclooxygenase 2-deficient mice. *Cell* 91(2):197–208.
31. Torban E, Wang HJ, Groulx N, Gros P (2004) Independent mutations in mouse Vangl2 that cause neural tube defects in looptail mice impair interaction with members of the Dishevelled family. *J Biol Chem* 279(50):52703–52713.
32. Devenport D, Fuchs E (2008) Planar polarization in embryonic epidermis orchestrates global asymmetric morphogenesis of hair follicles. *Nat Cell Biol* 10(11):1257–1268.
33. Kallay LM, McNickle A, Brennwald PJ, Hubbard AL, Braiterman LT (2006) Scribble associates with two polarity proteins, Lgl2 and Vangl2, via distinct molecular domains. *J Cell Biochem* 99(2):647–664.
34. Yoshihara K, et al. (2011) Phosphorylation state regulates the localization of Scribble at adherens junctions and its association with E-cadherin-catenin complexes. *Exp Cell Res* 317(4):413–422.
35. Hogan BL (1996) Bone morphogenetic proteins: Multifunctional regulators of vertebrate development. *Genes Dev* 10(13):1580–1594.
36. Ingham PW (1998) Transducing Hedgehog: The story so far. *EMBO J* 17(13):3505–3511.
37. Massagué J, Chen YG (2000) Controlling TGF-beta signaling. *Genes Dev* 14(6):627–644.
38. Paria BC, et al. (2001) Cellular and molecular responses of the uterus to embryo implantation can be elicited by locally applied growth factors. *Proc Natl Acad Sci USA* 98(3):1047–1052.
39. Lee KY, et al. (2007) Bmp2 is critical for the murine uterine decidual response. *Mol Cell Biol* 27(15):5468–5478.
40. Perez VA, et al. (2011) BMP promotes motility and represses growth of smooth muscle cells by activation of tandem Wnt pathways. *J Cell Biol* 192(1):171–188.
41. González-Sancho JM, et al. (2013) Functional consequences of Wnt-induced dishevelled 2 phosphorylation in canonical and noncanonical Wnt signaling. *J Biol Chem* 288(13):9428–9437.
42. Deng W, et al. (2016) p53 coordinates decidual sestrin 2/AMPK/mTORC1 signaling to govern parturition timing. *J Clin Invest* 126(8):2941–2954.
43. Foldynová-Trantírková S, et al. (2010) Breast cancer-specific mutations in CK1epsilon inhibit Wnt/beta-catenin and activate the Wnt/Rac1/JNK and NFAT pathways to decrease cell adhesion and promote cell migration. *Breast Cancer Res* 12(3):R30.
44. Nishita M, et al. (2010) Ror2/Frizzled complex mediates Wnt5a-induced AP-1 activation by regulating Dishevelled polymerization. *Mol Cell Biol* 30(14):3610–3619.
45. Schwarz-Romond T, Merrifield C, Nichols BJ, Bienz M (2005) The Wnt signalling effector Dishevelled forms dynamic protein assemblies rather than stable associations with cytoplasmic vesicles. *J Cell Sci* 118(Pt 22):5269–5277.
46. Schwarz-Romond T, Metcalfe C, Bienz M (2007) Dynamic recruitment of axin by Dishevelled protein assemblies. *J Cell Sci* 120(Pt 14):2402–2412.
47. Zhang H, et al. (2015) The homologous genes Vangl1 and Vangl2 are required for embryo implantation in the uterus of mice during early pregnancy. *Gene* 555(2):140–149.
48. Hoversland RC, Weitlauf HM (1981) The volume of uterine fluid in 'implanting' and 'delayed implanting' mice. *J Reprod Fertil* 62(1):105–109.
49. Dunlap KA, et al. (2011) Postnatal deletion of Wnt7a inhibits uterine gland morphogenesis and compromises adult fertility in mice. *Biol Reprod* 85(2):386–396.
50. Botchkarev VA, et al. (1999) Noggin is a mesenchymally derived stimulator of hair-follicle induction. *Nat Cell Biol* 1(3):158–164.
51. Paria BC, Zhao X, Das SK, Dey SK, Yoshinaga K (1999) Zonula occludens-1 and E-cadherin are coordinately expressed in the mouse uterus with the initiation of implantation and decidualization. *Dev Biol* 208(2):488–501.
52. Hagemann AI, et al. (2014) In vivo analysis of formation and endocytosis of the Wnt/β-catenin signaling complex in zebrafish embryos. *J Cell Sci* 127(Pt 18):3970–3982.
53. Smalley MJ, et al. (1999) Interaction of axin and Dvl-2 proteins regulates Dvl-2-stimulated TCF-dependent transcription. *EMBO J* 18(10):2823–2835.
54. Axelrod JD, Miller JR, Shulman JM, Moon RT, Perrimon N (1998) Differential recruitment of Dishevelled provides signaling specificity in the planar cell polarity and Wingless signaling pathways. *Genes Dev* 12(16):2610–2622.
55. Hertig AT, Rock J, Adams EC (1956) A description of 34 human ova within the first 17 days of development. *Am J Anat* 98(3):435–493.
56. Nikas G (1999) Pinopodes as markers of endometrial receptivity in clinical practice. *Hum Reprod* 14(Suppl 2):99–106.
57. Peter D, Marcella B (2008) The fine structure of the mature human endometrium. *The Endometrium: Molecular, Cellular, Clinic Perspectives*, eds Aplin JD, Fazleabas AT, Glasser SR, Giudice LC (Informa Healthcare, London) 2nd Ed, pp 46–65.
58. Shi D, et al. (2014) Celsr1 is required for the generation of polarity at multiple levels of the mouse oviduct. *Development* 141(23):4558–4568.
59. Ross AJ, et al. (2005) Disruption of Bardet-Biedl syndrome ciliary proteins perturbs planar cell polarity in vertebrates. *Nat Genet* 37(10):1135–1140.
60. Enders AC, Welsh AO, Schlafke S (1985) Implantation in the rhesus monkey: Endometrial responses. *Am J Anat* 173(3):147–169.
61. Faiz AS, Ananth CV (2003) Etiology and risk factors for placenta previa: An overview and meta-analysis of observational studies. *J Matern Fetal Neonatal Med* 13(3):175–190.
62. Lam CM, Wong SF, Chow KM, Ho LC (2000) Women with placenta praevia and antepartum haemorrhage have a worse outcome than those who do not bleed before delivery. *J Obstet Gynaecol* 20(1):27–31.
63. Uhlén M, et al. (2015) Proteomics. Tissue-based map of the human proteome. *Science* 347(6220):1260419.
64. Miyoshi H, Ajima R, Luo CT, Yamaguchi TP, Stappenbeck TS (2012) Wnt5a potentiates TGF-β signaling to promote colonic crypt regeneration after tissue injury. *Science* 338(6103):108–113.
65. Soyal SM, et al. (2005) Cre-mediated recombination in cell lineages that express the progesterone receptor. *Genesis* 41(2):58–66.
66. Chen Z, et al. (2016) cAMP/CREB-regulated LINC00473 marks LKB1-inactivated lung cancer and mediates tumor growth. *J Clin Invest* 126(6):2267–2279.
67. Ma X, et al. (2011) Decidual cell polyploidization necessitates mitochondrial activity. *PLoS One* 6(10):e26774.